

ROBUST DIFFERENTIAL STEERING CONTROL SYSTEM FOR AN INDEPENDENT FOUR WHEEL DRIVE ELECTRIC VEHICLE

Muhammad Arshad Khan¹⁾, Muhammad Faisal Aftab²⁾, Ejaz Ahmed¹⁾ and Iljoong Youn^{1)*}

¹⁾School of Mechanical and Aerospace Engineering, ReCAPT, Gyeongsang National University, Gyeongnam 52828, Korea

²⁾Department of Engineering Cybernetics, Norwegian University of Science and Technology, Trondheim NO-7491, Norway

(Received 27 October 2017; Revised 6 June 2018; Accepted 24 July 2018)

ABSTRACT—This research investigates a robust differential steering control system (DSCS) for an independent four wheel drive electric vehicle (EV). The DSCS will maneuver the independently actuated (IA) four wheel drive EV without the help of any conventional steering mechanism (CSM) via the input torque of the four wheels. The differential angular rotation speed between left and right wheels is used to generate the CSM effects. The DSCS is designed using the linear model of the vehicle with linear tire dynamics and is tested in simulations using a nonlinear vehicle model with nonlinear tire dynamics. The proposed DSCS is a combination of forward speed and yaw rate controllers, designed using the robust H_∞ control methodology. The effectiveness of the proposed robust controller is analyzed by comparing the performance of the all-wheel drive (AWD), the rear wheel drive (RWD), and the front wheel drive (FWD) vehicles during simulations. The simulation results indicate that the proposed system can successfully maneuver the vehicle under different driving conditions by tracking the desired parameters without the use of any CSM.

KEY WORDS : Vehicle dynamics, Steering control, Yaw tracking, Nonlinear vehicle model, Four-wheel-steering control, Differential steering control, Four wheel drive, Electric vehicle, H_∞ controller

1. INTRODUCTION

Recent years have witnessed an increasing demand for EV. Due to the development of the advanced technology for safety and high mobility the environment friendly EV has become a prime focus of research in the automobile industry (Chen and Li, 2014). With the introduction of new technology and new control inputs, EV is considered to be more easily controllable as compared to the internal combustion engine vehicles (ICEV) (Hori, 2004). The emergence of the independently actuated (IA) drive in EV opened many new research areas for the improvement of the maneuverability and active safety (Li *et al.*, 2015; Ono *et al.*, 2006; Wang *et al.*, 2011, 2016). The in-wheel IA motors, can result in fast and accurate torque distribution and more effective actuation for the motion control of the vehicle (Xiong and Yu, 2009; Zhang *et al.*, 2014a, 2014b). Numerous studies have revealed that by making full use of the additional control capabilities, the EV maneuverability, stability, and safety can be considerably improved (Jang *et al.*, 2017; Wu *et al.*, 2018; Yin *et al.*, 2015).

Differential steering control system (DSCS) is a novel steering mechanism for the IA EV. In conventional ICEV, a steering mechanism is one of the main components of the

vehicle and it is considered to be indispensable for maneuvering the vehicle. However, by using DSCS which utilizes the merits of independently controlled in-wheel motors of the EV the CSM can be replaced.

DSCS utilizes the concept of differential drive where the steering angle is generated by the difference of angular velocity of the wheels using IA in-wheel motors of the vehicle. Several previous researches have utilized the concept of differential drive for the better control and navigation of mobile robots (Chen and Kuo, 2014; Kozłowski and Pazderski, 2004; Yi *et al.*, 2009; Yu *et al.*, 2010). However, the previous researches considered the differential drive as the additional power source to assist the steering and driving maneuvers. Wu *et al.* (2013) introduced differential speed steering control for four wheels independent wheel drive EV considering only slow speed vehicles. Recently Hu *et al.* (2016) introduced a path following control for IA autonomous vehicles with differential steering in the case of the complete failure of the active front-wheel steering system. However this controller become active once the conventional CSM fails, furthermore this controller utilizes only front wheel as the sole steering input.

This work is aimed at replacing the CSM with more flexible DSCS. The proposed robust H_∞ controller is designed using the linear model of the vehicle dynamics,

*Corresponding author. e-mail: iyoun@gnu.ac.kr

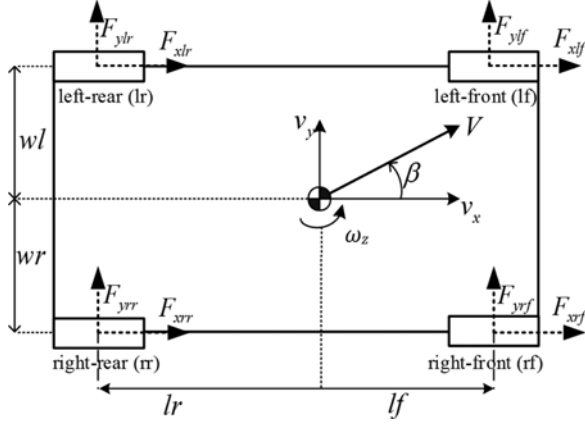


Figure 1. Vehicle model.

computed at the varying operating conditions. The DSCS performance is verified using a more detailed nonlinear vehicle model with nonlinear tire dynamics. Simulation results show that the DSCS can be used independently to control the vehicle maneuvers without the use of CSM. It is further verified that the DSCS is effective in tracking the desired yaw rate while maintaining the forward speed during the maneuver. The permanence of the designed DSCS is compared for FWD, RWD and AWD cases.

The main contributions of this paper are 1) Replacing the CSM with DSCS which utilizes the already available IA in wheel motors as control input. 2) A comparison of DSCS for FWD, RWD and AWD IA EV.

The rest of this paper is organized as follows. Section 2 presents the mathematical models of the tire and vehicle. Section 3 describes the design procedure for the robust H_∞ controllers. Simulations results using a high fidelity nonlinear vehicle model are discussed in Section 4, followed by conclusion.

2. MATHEMATICAL MODELING OF THE VEHICLE

This section explains the mathematical models used in this paper. The vehicle considered here is an electrical vehicle with four IA in-wheel motors; each motor speed can be controlled independently. The nonlinear vehicle model, as shown in Figure 1, includes three states as the vehicle total velocity (V), side-slip angle (β) and yaw rate (ω_z) of the body while the remaining four states are related to the angular rotation (ω_{ij}) of the four wheels. In this vehicle model all wheels are considered to be connected without any steering mechanism therefore the steering angle (δ) at the front and rear wheels is zero. The suspension dynamics is also neglected in this research. In this paper, a linear model is utilized for the design of the controller while a nonlinear vehicle model is utilized for the implementation and testing of the proposed controller.

2.1. Nonlinear Model of the Vehicle

The dynamic equations of the nonlinear vehicle model without steering angle can be derived as

$$m\dot{V} = (F_{xlf} + F_{xrf} + F_{xlr} + F_{xrr}) \cos(\beta) + (F_{ylf} + F_{yrf} + F_{ylr} + F_{yrr}) \sin(\beta) \quad (1)$$

$$m\dot{\beta} = \frac{1}{V} [(F_{ylf} + F_{yrf} + F_{ylr} + F_{yrr}) \cos(\beta) - (F_{xlf} + F_{xrf} + F_{xlr} + F_{xrr}) \sin(\beta)] - m\omega_z \quad (2)$$

$$J_z \dot{\omega}_z = l_f (F_{ylf} + F_{yrf}) - l_r (F_{ylr} + F_{yrr}) + w_r (F_{xrf} + F_{xrr}) - w_l (F_{xlf} + F_{xlr}) \quad (3)$$

$$J_{wij} \dot{\omega}_{ij} = -F_{xij} r_{ij} + \tau_{bij} \quad (4)$$

Where m is the mass of the vehicle, (l_f , l_r , w_l , and w_r) are the length from the center of the mass (COM) to the front, rear, left, and right tires center respectively, (J_z) is the moment of inertia about the vertical axis, (F_{xij}) are the longitudinal and (F_{yij}) are the lateral tire forces at each wheel. The variables (J_{wij} , r_{ij} , τ_{bij}) are the rotational inertia, effective wheel radius and input torque of the individual wheels respectively. The variable ($i = l, r$) corresponds to left and right respectively and the variable ($j = f, r$) corresponds to front and rear respectively.

2.2. Tire Model

Tire model is one of basic building block of every vehicle dynamic simulation. Tire model produces the forces required to drive the simulation/model. Two different tire models are utilized in this study as the means to acquire the tire forces, (F_{xij} and F_{yij}). The linear tire model simply calculates the forces as the product of the cornering (or longitudinal) tire stiffness and the side-slip angle (or longitudinal slip ratio), whereas the pacejka tire model plugs in the experimentally chosen constants into Pacejka Magic Formula (Bakker *et al.*, 1987).

In this research, the linear tire model is used with the nonlinear vehicle model for the generation of the linearized vehicle model while the nonlinear tire model is used with nonlinear vehicle model for controller performance validation during simulations.

2.2.1. Non-linear tire model of the vehicle

Nonlinear tire forces (F_{xij} , F_{yij}) which are used in the mentioned vehicle model, are calculated as function of tire slip using Pacejkas Magic Formula as explained by Bakker *et al.* (1987). The total friction coefficient at each wheel is calculated as a function of total slip using magic formula as

$$\mu_{ij}(s_{ij}) = D \sin(C \arctan(Bs_{ij})) \quad (5)$$

Where the resultant tire slip (s_{ij}) is calculated as

$$s_{ij} = \sqrt{s_{xij}^2 + s_{yij}^2} \quad (6)$$

The theoretical longitudinal slips (s_{xij}) and the lateral slips

(s_{yij}) are calculated as

$$s_{xij} = \frac{V_{xij} - \omega_{ij} r_{ij}}{\omega_{ij} r_{ij}}, \quad s_{yij} = \frac{V_{yij}}{\omega_{ij} r_{ij}} = (1 + s_{xij}) \tan(\alpha_{ij}) \quad (7)$$

Where (V_{xij} , V_{yij}) are the longitudinal and lateral components of the vehicle body velocity vector at the corresponding wheels. The slip angle at each wheel is calculated as

$$\tan(\alpha_{ij}) = \frac{V_{yij}}{V_{xij}} \quad (8)$$

Using the friction circle equation, the friction coefficients components in the longitudinal and lateral direction are given as

$$\mu_{xij} = -\frac{s_{xij}}{s_{ij}} \mu_{ij}(s_{ij}), \quad \mu_{yij} = -\frac{s_{yij}}{s_{ij}} \mu_{ij}(s_{ij}) \quad (9)$$

By utilizing (F_{zij}) as the vertical force on each of the four wheels, the longitudinal and lateral tire forces can be calculated as

$$F_{xij} = \mu_{xij} F_{zij}, \quad F_{yij} = \mu_{yij} F_{zij} \quad (10)$$

2.2.2. Linear tire model of the vehicle

The mathematical equations of the linear tire model can be written as

$$F_{xij} = C_{xij} \alpha_{xij}, \quad F_{yij} = C_{yij} \alpha_{yij} \quad (11)$$

Where (C_{xij}) is the longitudinal tire stiffness constant, (C_{yij}) is the tire cornering stiffness constant, (α_{xij}) is the longitudinal slip ratio and (α_{yij}) is the side-slip angle. The constant (C_{xij}) and (C_{yij}) are used from the work by Youn *et al.* (2015), while (α_{xij}) and (α_{yij}) can be calculated as

$$\alpha_{xij} = \frac{\omega_{ij} r_{ij} - V_{xij}}{\max |V_{xij}, \omega_{ij} r_{ij}|}, \quad \alpha_{yij} = \frac{-V_{yij}}{V_{xij}} \quad (12)$$

The longitudinal and lateral velocities of the individual wheels are calculated as

$$\begin{bmatrix} V_{xrf} \\ V_{xlf} \\ V_{xlr} \\ V_{xrr} \end{bmatrix} = \begin{bmatrix} V_x \\ V_x \\ V_x \\ V_x \end{bmatrix} + \begin{bmatrix} wr \\ -wl \\ -wl \\ wr \end{bmatrix} \omega_z \quad (13)$$

$$\begin{bmatrix} V_{yrf} \\ V_{ylf} \\ V_{ylr} \\ V_{yrr} \end{bmatrix} = \begin{bmatrix} V_y \\ V_y \\ V_y \\ V_y \end{bmatrix} + \begin{bmatrix} lf \\ lf \\ -lr \\ -lr \end{bmatrix} \omega_z$$

The longitudinal and lateral velocities (V_x and V_y) at COM is calculated as

$$V_x = V \cos(\beta), \quad V_y = V \sin(\beta), \quad (14)$$

2.3. Linear Model of the Vehicle

Using the linear tire model, the nonlinear model of the vehicle is linearized using Taylor series approximation at the equilibrium points V^* , β^* , ω_z^* and ω_{ij}^* . The nonlinear model is linearized at varying operating conditions with $2 \leq V^* \leq 30$ m/sec and $0 \leq \omega_z^* \leq 30$ θ /sec, the value of β^* is kept at its corresponding equilibrium condition. The steady state values for the angular rotation of the individual wheels is calculated as

$$\omega_{ij}^* = V/r_{ij} \quad (15)$$

The linear model can be written as

$$\dot{X} = AX + BU \quad (16)$$

where the Jacobean state space matrices (A) and (B) can be derived mathematically as

$$A = \begin{bmatrix} \frac{\partial \dot{V}}{\partial V} & \frac{\partial \dot{V}}{\partial \beta} & \frac{\partial \dot{V}}{\partial \omega_z} & \frac{\partial \dot{V}}{\partial \omega_{lf}} & \frac{\partial \dot{V}}{\partial \omega_{rf}} & \frac{\partial \dot{V}}{\partial \omega_{lr}} & \frac{\partial \dot{V}}{\partial \omega_{rr}} \\ \frac{\partial \dot{\beta}}{\partial V} & \frac{\partial \dot{\beta}}{\partial \beta} & \frac{\partial \dot{\beta}}{\partial \omega_z} & \frac{\partial \dot{\beta}}{\partial \omega_{lf}} & \frac{\partial \dot{\beta}}{\partial \omega_{rf}} & \frac{\partial \dot{\beta}}{\partial \omega_{lr}} & \frac{\partial \dot{\beta}}{\partial \omega_{rr}} \\ \frac{\partial \dot{\omega}_z}{\partial V} & \frac{\partial \dot{\omega}_z}{\partial \beta} & \frac{\partial \dot{\omega}_z}{\partial \omega_z} & \frac{\partial \dot{\omega}_z}{\partial \omega_{lf}} & \frac{\partial \dot{\omega}_z}{\partial \omega_{rf}} & \frac{\partial \dot{\omega}_z}{\partial \omega_{lr}} & \frac{\partial \dot{\omega}_z}{\partial \omega_{rr}} \\ \frac{\partial \dot{\omega}_{lf}}{\partial V} & \frac{\partial \dot{\omega}_{lf}}{\partial \beta} & \frac{\partial \dot{\omega}_{lf}}{\partial \omega_z} & \frac{\partial \dot{\omega}_{lf}}{\partial \omega_{lf}} & \frac{\partial \dot{\omega}_{lf}}{\partial \omega_{rf}} & \frac{\partial \dot{\omega}_{lf}}{\partial \omega_{lr}} & \frac{\partial \dot{\omega}_{lf}}{\partial \omega_{rr}} \\ \frac{\partial \dot{\omega}_{rf}}{\partial V} & \frac{\partial \dot{\omega}_{rf}}{\partial \beta} & \frac{\partial \dot{\omega}_{rf}}{\partial \omega_z} & \frac{\partial \dot{\omega}_{rf}}{\partial \omega_{lf}} & \frac{\partial \dot{\omega}_{rf}}{\partial \omega_{rf}} & \frac{\partial \dot{\omega}_{rf}}{\partial \omega_{lr}} & \frac{\partial \dot{\omega}_{rf}}{\partial \omega_{rr}} \\ \frac{\partial \dot{\omega}_{lr}}{\partial V} & \frac{\partial \dot{\omega}_{lr}}{\partial \beta} & \frac{\partial \dot{\omega}_{lr}}{\partial \omega_z} & \frac{\partial \dot{\omega}_{lr}}{\partial \omega_{lf}} & \frac{\partial \dot{\omega}_{lr}}{\partial \omega_{rf}} & \frac{\partial \dot{\omega}_{lr}}{\partial \omega_{lr}} & \frac{\partial \dot{\omega}_{lr}}{\partial \omega_{rr}} \\ \frac{\partial \dot{\omega}_{rr}}{\partial V} & \frac{\partial \dot{\omega}_{rr}}{\partial \beta} & \frac{\partial \dot{\omega}_{rr}}{\partial \omega_z} & \frac{\partial \dot{\omega}_{rr}}{\partial \omega_{lf}} & \frac{\partial \dot{\omega}_{rr}}{\partial \omega_{rf}} & \frac{\partial \dot{\omega}_{rr}}{\partial \omega_{lr}} & \frac{\partial \dot{\omega}_{rr}}{\partial \omega_{rr}} \end{bmatrix}_{(V^*, \beta^*, \omega_z^*, \omega_{lf}^*, \omega_{rf}^*, \omega_{lr}^*, \omega_{rr}^*)} \quad (17)$$

$$B = \begin{bmatrix} \frac{\partial \dot{V}}{\partial \tau_{lf}} & \frac{\partial \dot{V}}{\partial \tau_{rf}} & \frac{\partial \dot{V}}{\partial \tau_{lr}} & \frac{\partial \dot{V}}{\partial \tau_{rr}} \\ \frac{\partial \dot{\beta}}{\partial \tau_{lf}} & \frac{\partial \dot{\beta}}{\partial \tau_{rf}} & \frac{\partial \dot{\beta}}{\partial \tau_{lr}} & \frac{\partial \dot{\beta}}{\partial \tau_{rr}} \\ \frac{\partial \dot{\omega}_z}{\partial \tau_{lf}} & \frac{\partial \dot{\omega}_z}{\partial \tau_{rf}} & \frac{\partial \dot{\omega}_z}{\partial \tau_{lr}} & \frac{\partial \dot{\omega}_z}{\partial \tau_{rr}} \\ \frac{\partial \dot{\omega}_{lf}}{\partial \tau_{lf}} & \frac{\partial \dot{\omega}_{lf}}{\partial \tau_{rf}} & \frac{\partial \dot{\omega}_{lf}}{\partial \tau_{lr}} & \frac{\partial \dot{\omega}_{lf}}{\partial \tau_{rr}} \\ \frac{\partial \dot{\omega}_{rf}}{\partial \tau_{lf}} & \frac{\partial \dot{\omega}_{rf}}{\partial \tau_{rf}} & \frac{\partial \dot{\omega}_{rf}}{\partial \tau_{lr}} & \frac{\partial \dot{\omega}_{rf}}{\partial \tau_{rr}} \\ \frac{\partial \dot{\omega}_{lr}}{\partial \tau_{lf}} & \frac{\partial \dot{\omega}_{lr}}{\partial \tau_{rf}} & \frac{\partial \dot{\omega}_{lr}}{\partial \tau_{lr}} & \frac{\partial \dot{\omega}_{lr}}{\partial \tau_{rr}} \\ \frac{\partial \dot{\omega}_{rr}}{\partial \tau_{lf}} & \frac{\partial \dot{\omega}_{rr}}{\partial \tau_{rf}} & \frac{\partial \dot{\omega}_{rr}}{\partial \tau_{lr}} & \frac{\partial \dot{\omega}_{rr}}{\partial \tau_{rr}} \end{bmatrix}_{(V^*, \beta^*, \omega_z^*, \omega_{lf}^*, \omega_{rf}^*, \omega_{lr}^*, \omega_{rr}^*)} \quad (18)$$

the states matrix X and the control inputs matrix U of the linear system can be written as

$$X = [V \quad \beta \quad \omega_z \quad \omega_{lf} \quad \omega_{rf} \quad \omega_{lr} \quad \omega_{rr}]^T, \quad (19)$$

$$U = [\tau_{lf} \quad \tau_{rf} \quad \tau_{lr} \quad \tau_{rr}]^T$$

2.4. Comparison of the Linear and Nonlinear Model of the Vehicle

In this section, the linear and nonlinear models of the vehicle are compared to check the validity of the linear models before they can be used for controller design. Both

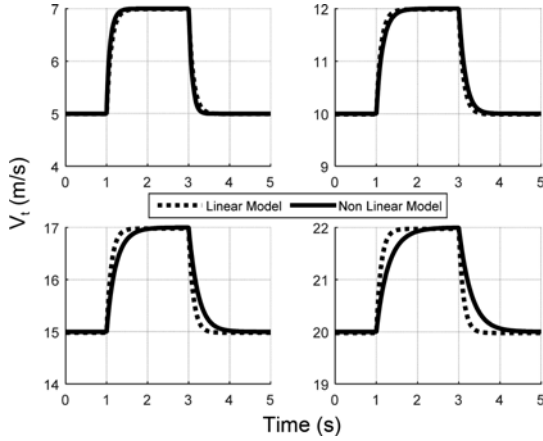


Figure 2. Total velocity based comparison of the linear and nonlinear vehicle models.

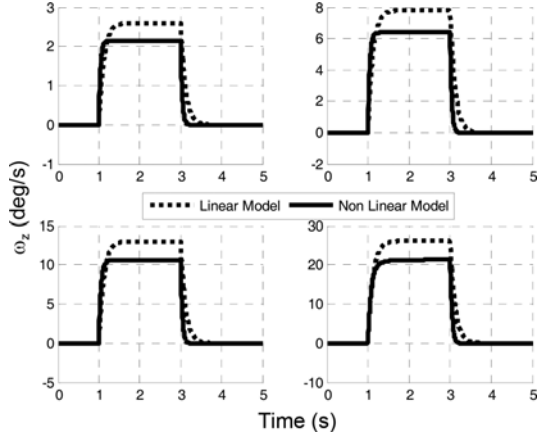


Figure 3. Yaw rate based comparison of the linear and nonlinear vehicle models.

of the models are excited at the steady state conditions using the same step inputs of the angular velocities of the four wheels. Figure 2 shows the comparison of the linear and nonlinear models at different equilibrium points corresponding to velocities of 5, 10, 15 and 20 m/sec respectively.

Similarly, Figure 3 shows the yaw rate comparison of the linear and nonlinear models at different equilibrium points corresponding to the constant speed of 8 m/sec and steering angle input of 1, 3, 5 and 10 degrees respectively. It is observed that the linear model follows the nonlinear model closely in transients and steady state conditions. Therefore, the linear model is suitable enough to be used for the controller design.

3. CONTROLLER DESIGN

This section discusses the design of the controllers used for the proposed DSCS. Figure 4 shows the main block diagram for the designed control system. The DSCS will be

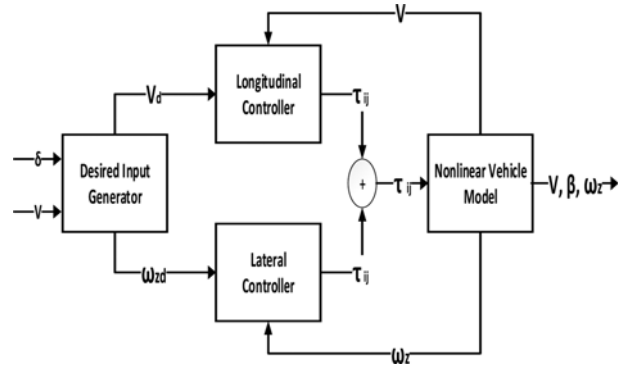


Figure 4. Control architecture for GSCS.

implemented in three stages. In first stage the desired yaw rate and desired speed is calculated using the inputs from the driver, in the second stage the robust H_∞ controller generates the desired wheel torques as the controller output and lastly in the third stage the combined torque of the four wheels are applied to the actual system/mathematical model. Using the linear models of the vehicle, two controllers (speed and yaw control) are designed using a robust H_∞ controller to ensure the effectiveness of the proposed control system under different driving conditions.

3.1. H_∞ Loop-shaping Design Procedure

The H_∞ loop-shaping design procedure adopted in this work is shown in Figure 5. The plant model G is appended with pre and post compensators W_1 , W_2 to form a shaped plant G_s .

The shaped plant can be written mathematically as

$$G_s = W_2 G W_1 \quad (20)$$

The robust H_∞ controller feedback control gain K_g is calculated using McFarlane and Glover technique (McFarlane and Glover, 1990) as

$$K_g = \begin{bmatrix} A + BF + \gamma^2 (L^T)^{-1} ZC^T (C + DF) & \gamma^2 (L^T)^{-1} ZC^T \\ B^T X & -D^T \end{bmatrix} \quad (21)$$

where

$$F = -S^{-1} (D^T C + B^T X), \quad L = (1 - \gamma^2) I + XZ \quad (22)$$

the stability property is robust if and only if the nominal

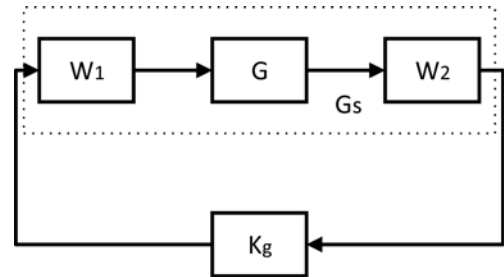


Figure 5. H_∞ shaped plant with controller.

feedback system is stable and

$$\gamma = \left\| \begin{bmatrix} K \\ I \end{bmatrix} (I - GK)^{-1} M^{-1} \right\|_{\infty} \leq \frac{1}{\varepsilon} \quad (23)$$

for a minimal state-space realization (A, B, C, D) of plant G, the variable Z is the unique positive definite solution of the following Algebraic Riccati Equation (ARE)

$$\begin{aligned} (A - BS^{-1}D^T C)Z + Z(A - BS^{-1}D^T C)^T \\ - ZC^T R^{-1} CZ + BS^{-1}B^T = 0 \end{aligned} \quad (24)$$

where $R = I + DD^T$ and $S = I + D^T D$ the variable X is the unique positive definite solution of the following ARE

$$\begin{aligned} (A - BS^{-1}D^T C)_T X + X(A - BS^{-1}D^T C) \\ + XBS^{-1}B^T X + C^T R^{-1} C = 0 \end{aligned} \quad (25)$$

3.2. H_{∞} Loop-shaping Parameters Selection

The controller design procedure involves selection of appropriate pre and post compensators (weights) $W1$ and $W2$ according to the criteria presented in Skogestad and Postlethwaite (1996) to achieve the desired loop shape in the frequency domain. The weights are selected such that objectives like reference tracking, disturbance rejection and robustness against noise can be achieved. The low frequency gain is increased in order to reject the disturbances and track the reference signals whereas a

Table 1. Controller parameters.

Parameter	Yaw rate	Velocity
Crossover (rad/s)	1.4	1.0
Gamma (γ)	1.69	2.2
S peak (M_s)	1.05	1.21
T peak (M_T)	1.01	1.26
Controller order	3	3

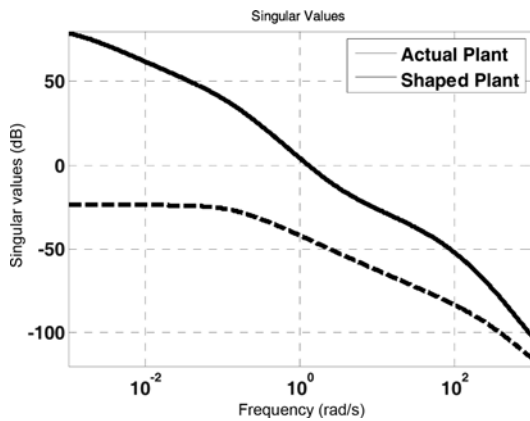


Figure 6. Frequency response of actual and shaped plant for velocity controller.

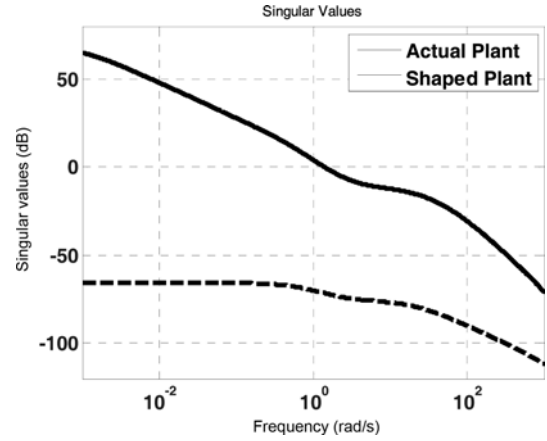


Figure 7. Frequency response of actual and shaped plant for yaw controller.

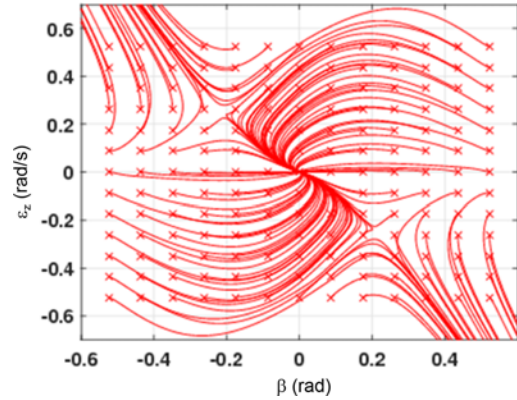


Figure 8. Phase portrait beta vs Yaw rate without controller.

higher roll off at the higher frequency ensures noise rejection and robustness against the un-modelled dynamics. Figures 6 and 7 shows the frequency response of the actual and the designed shaped plants for the speed and yaw controllers respectively.

Small values of sensitivity (S) and complimentary sensitivity (T) peaks ensure the robustness of the designed system. Controller order is reduced using the Hankel-norm reduction technique (Glover, 1984). The design parameters are listed in Table 1.

3.3. H_{∞} Stability Analysis

In this section, the stability of the used vehicle models with H_{∞} controller is analysed graphically. To keep the vehicle stable under different operating conditions, It is required to identify the operating envelope that can be achieved. Phase portrait analysis is one of the useful graphical methods for the identification of unstable regions reachable through different input. In this research, the phase portrait is generated by simulating the nonlinear vehicle model for the range of initial conditions of yaw rate and side-slip angle

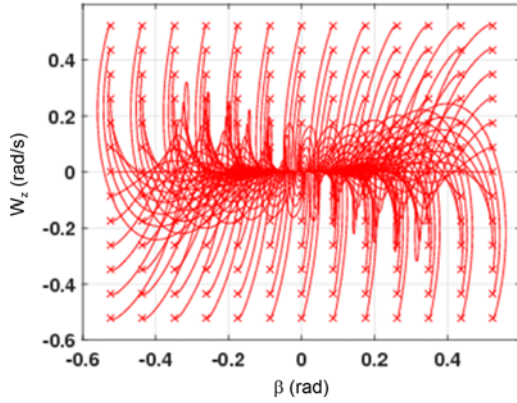


Figure 9. Phase portrait beta vs Yaw rate with controller.

while keeping the input velocity constant at 20 m/sec and steering angle input at zero. The resultant trajectories are plotted in (β, ω_z) plane.

Figure 8 shows the phase portrait of the model without controller, which shows the existence of three equilibrium conditions: a stable equilibrium at the center of the plot corresponding to straight line driving and two unstable drift equilibria. The unstable equilibria corresponds to the initial conditions where the yaw rate and side-slip angle have high magnitude and opposite signs. Figure 9 shows the phase portrait of the same model under same conditions with controller, one can see that the DSCS also improves the stability region of the system by converging the unstable trajectories to origin.

Moreover the designed controller gives stable closed loop system for all the linear models that encompass a wide range of the operating conditions.

Figures 10 and 11 shows the step responses of all linearized velocity and yaw rate models with controller respectively, one can see that all of the models are following the step command. It is observed that some of the yaw rate models have slow response, whereas velocity models have large overshoot, however this problem can be

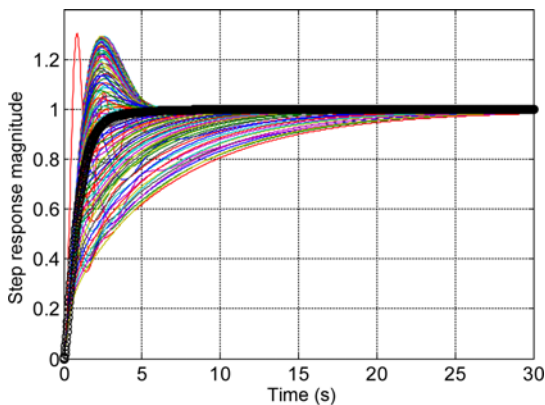


Figure 10. Step responses for the velocity models with controller.

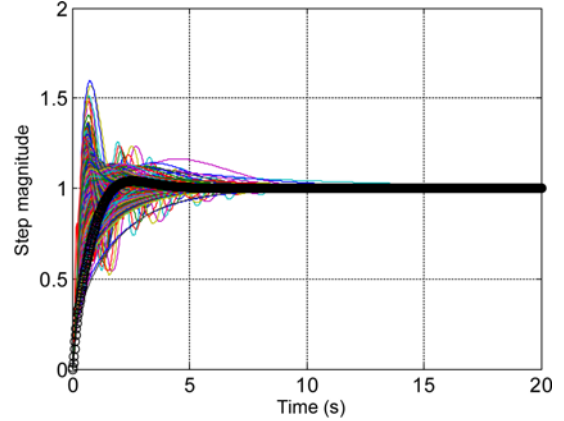


Figure 11. Step responses for the yaw rate models with controller.

Table 2. Vehicle and tire parameters.

Variable	Data	Variable	Data
m (kg)	850	h (m)	0.5
J_z (kgm ²)	1400	J_w (kgm ²)	0.6
l_f (m)	1.5	l_r (m)	0.9
r_{ij} (m)	0.311	B-dry	10
C-dry	1.9	D-dry	1
B-ice	1.3	C-ice	0.6
D-ice	0.6		
C_{xij}	10000	C_{yij}	15000

tuned by incorporating gain scheduling instead of one gain for all operating ranges.

4. SIMULATION RESULTS

In this section, three simulation scenarios corresponding to the driving maneuvers of a J-turn and a lane-change, are considered with different sets of vehicle velocity, road conditions and desired yaw rate. In the presented scenarios, the main control objective is to show that IA EV is maneuvered using DSCS only and without the help of any CSM. Both simulations are performed using the high-fidelity nonlinear vehicle model with nonlinear tire dynamics. The road condition used in the simulations are taken to be an icy road condition and an external yaw moment saturation limit is assumed to be 2.0 KNm (Du *et al.*, 2010). To highlight the effectiveness of the presented idea and controller, in each scenario the controller is tested with three different subcases of FWD, RWD, and AWD IA EV. The vehicle and tire model parameters are listed in Table 2. The desired yaw rate is calculated using formulation in Wong (1993) as

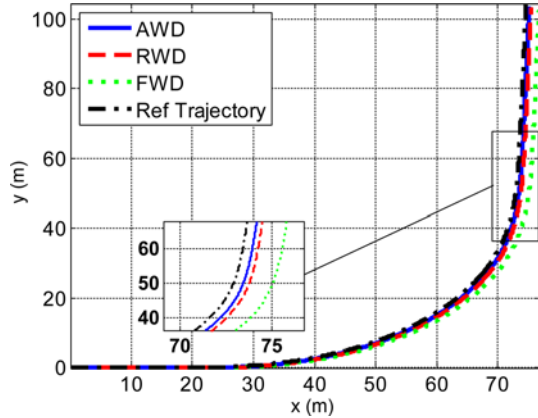


Figure 12. Final trajectories comparison results in the case of J-turn simulations.

$$\omega_{zd} = \frac{V_x}{(l_f + l_r) + qV_x^2} \delta, \quad q = \frac{m(l_r - l_f)}{2(l_r + l_f)C_y} \quad (26)$$

4.1. J-turn Scenario Simulation

In the first scenario, the simulation is initialized with the actual driver inputs corresponding to the vehicle total velocity of ($V = 13$ m/sec) and steering angle input profile corresponding to the vehicle trajectory as shown in Figure 12.

This scenario corresponds to a slow moving vehicle with big steering angle to track a challenging J-turn path. The control objectives are to track the input velocity and desired yaw rate simultaneously by using only the angular velocities of the four wheels.

From Figure 12, one can see that the presented DSCS controller was able to maneuver the vehicle for all of the three cases without the use of any CSM but the AWD IA EV shows the best performance for tracking the desired trajectory.

Figure 13, shows the yaw rate tracking performance comparison of the controller for the three sub cases of AWD, RWD, and FWD. The yaw rate tracking performance

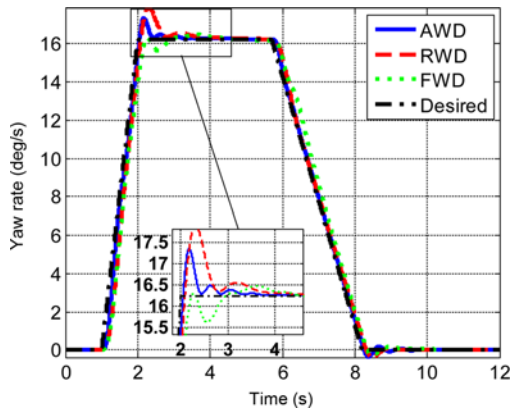


Figure 13. Yaw rate comparison results in the case of J-turn simulations.

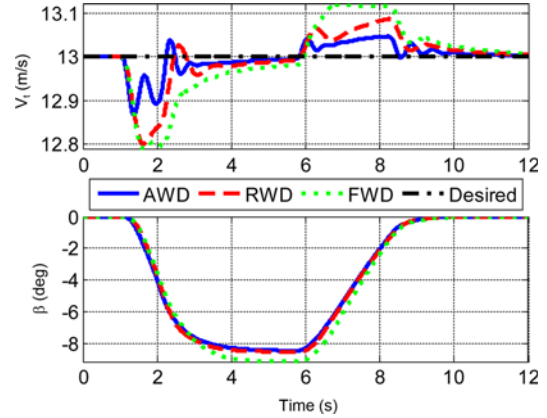


Figure 14. Vehicle total velocity, side-slip angle comparison results in the case of J-turn simulations.

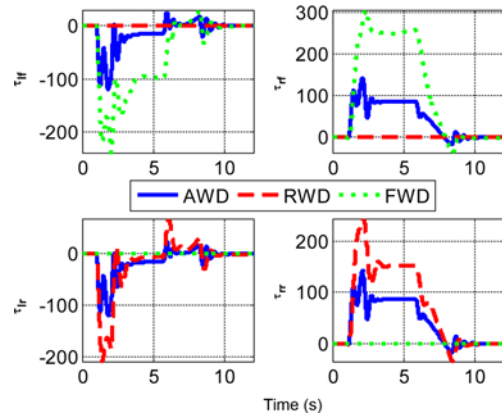


Figure 15. Control inputs comparison results in the case of J-turn simulations.

of the DSCS controller using an AWD EV shows the best results with lower overshoot and small settling time as compared to RWD and FWD.

Similar results are also observed in the case of total velocity tracking as shown in Figure 14, again AWD EV shows the best performance for the input velocity tracking as compared to RWD and FWD. Figure 14 also shows the comparison of the side-slip angle results generated during simulation, DSCS with AWD produced smaller side-slip angle as compare to RWD and FWD.

Figure 15 shows the comparison of the control inputs generated during J-turn maneuver for the three cases, it can be seen that in the case of AWD vehicle the controller stabilized the tracking problem with minimum and equally distributed control inputs as the forces are equally allocated to the four wheels of the vehicle. From the control input profile of the RWD and FWD it is evident that, in order to achieve the same control objective high torques of the corresponding rear and front wheels are required.

Figure 16 shows the individual wheel's slip generated for the three sub cases. From this figure it is evident that in

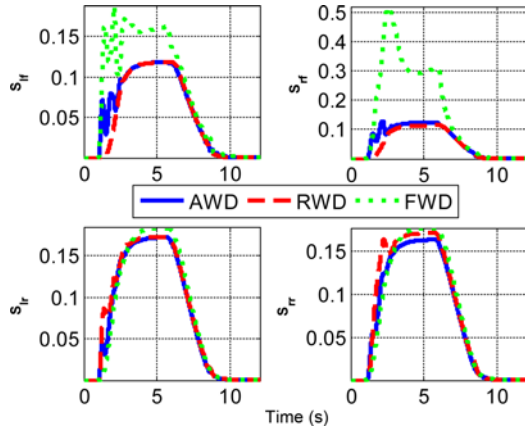


Figure 16. Wheel Slip comparison results in the case of J-turn simulations.

icy conditions due to the limited friction forces between road surface and tires of the vehicle, the generated slip between the road and the wheels is very high, especially the slip ratio for the FWD case is the worse.

From the comparison of the RWD and FWD in the case of icy road conditions, it is also observed that RWD tracking and control input distribution performance is better than FWD, the reason for the difference in the FWD and RWD with limited friction is the COM of the vehicle.

From the vehicle parameters listed in Table 2, it can be seen that $l_f > l_r$, therefore the rear wheels in case of RWD will have more effects on the system performance as compared to the front wheels in case of FWD due to the large vertical loads at the rear wheels.

This phenomenon can be verified by comparing the results of the J-turn simulation for FWD case with $l_f > l_r$, $l_f = l_r$ and $l_f < l_r$ as shown in Figure 17.

It can be seen that FWD with understeer condition i.e. COM at the front produces better results as compared to other two cases. Consequently it can be stated that in icy condition cases the COM plays a critical role in the

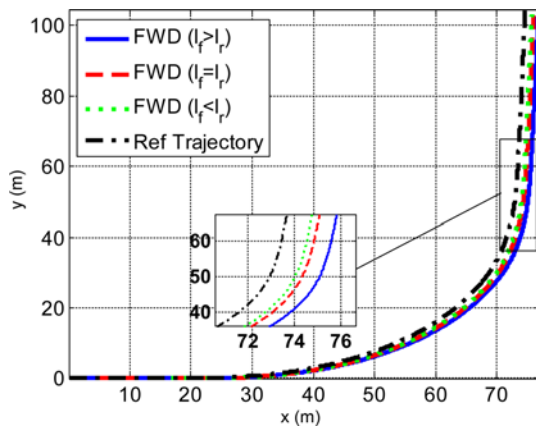


Figure 17. Final trajectories comparison for FWD in the case of J-turn simulations.

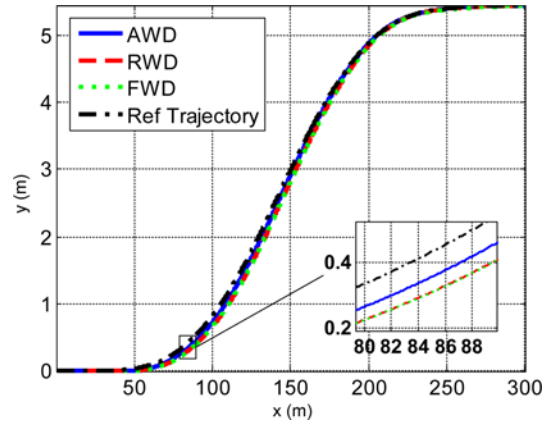


Figure 18. Final trajectories comparison results in the case of lane change simulations icy conditions.

stability of the vehicle and in cases where $l_f = l_r$, the performance of FWD and RWD EV will be same. In addition the AWD EV will always produce best performance due to additional control forces and equal distribution of the available tire forces.

4.2. Lane Change Scenario Simulation Icy Road Conditions

In the second scenario, the trajectory corresponding to a lane change maneuver at 25 m/sec speed is considered again with icy road conditions. The trajectory profile is shown in Figure 18. This scenario corresponds to fast moving vehicle with small steering angle to simulate a lane change trajectory with same control objectives.

The yaw rate response for three cases AWD, RWD and FWD are shown in Figure 19. It is evident from the results that the desired maneuver is achieved without use of CSM. Here again, similar to the J-turn case, the AWD vehicle gives the best performance.

Similar results are achieved for the velocity tracking with AWD outperforming the other two cases as shown in Figure 20. Side-slip angle produced in case of AWD is also

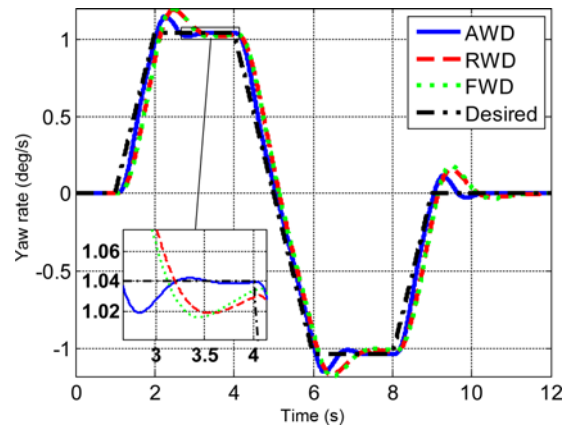


Figure 19. Yaw rate comparison results in the case of lane change simulations icy conditions.

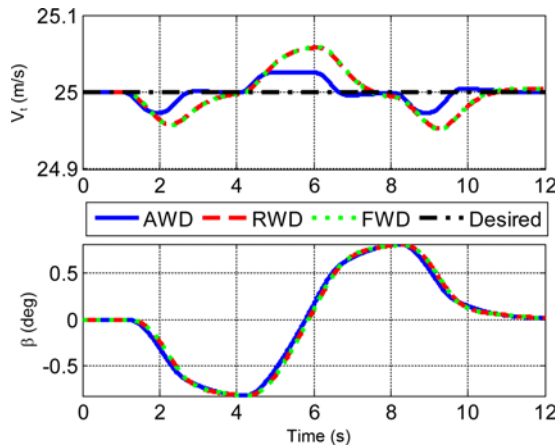


Figure 20. Vehicle total velocity, side-slip angle comparison results in the case of lane change simulations icy conditions.

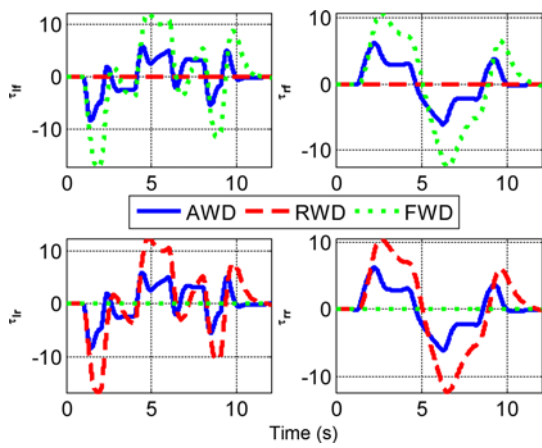


Figure 21. Control inputs comparison results in the case of lane change simulations icy conditions.

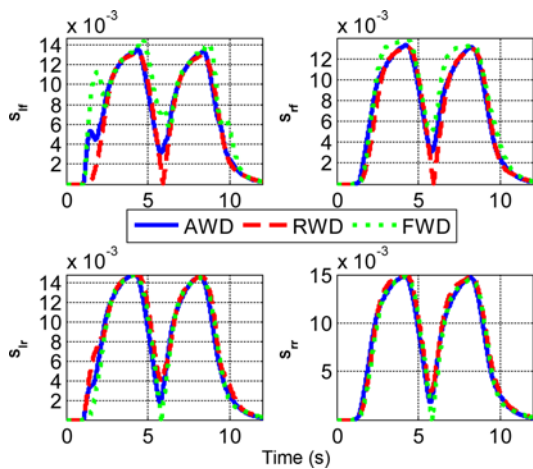


Figure 22. Wheel Slip comparison results in the case of lane change simulations icy conditions.

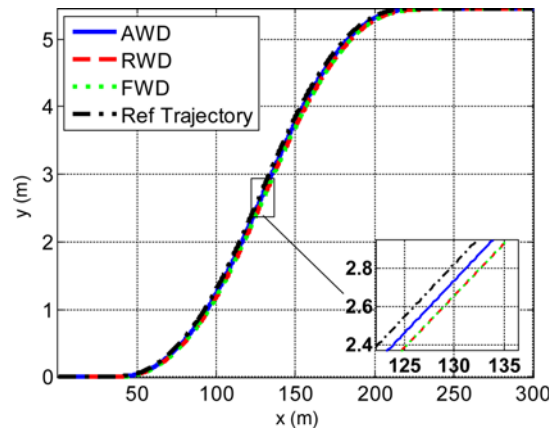


Figure 23. Final trajectories comparison results in the case of lane change simulations dry conditions.

lower than other cases.

The control inputs have similar behavior as observed in the case of J-turn maneuver as shown in Figure 21.

Figure 22 shows the individual wheel's slip generated for the three sub cases. In lane change scenario due to small desired yaw rate the total slip ratio is much smaller as compared to the J-turn case. Due to small wheels slips the controller can efficiently tract the input velocity and yaw rate with minimum control inputs.

4.3. Lane Change Scenario Simulation Dry Road Conditions

In the third scenario, the trajectory corresponding to a lane change maneuver at 25 m/sec speed is considered but with dry road conditions to further verify the performance difference of FWD and RWD EV. The trajectory profile is shown in Figure 23. From this figure it can be noted that although AWD produced the best results, the FWD and RWD trajectories produced similar performance. This is due to the availability of good friction forces due to dry road conditions.

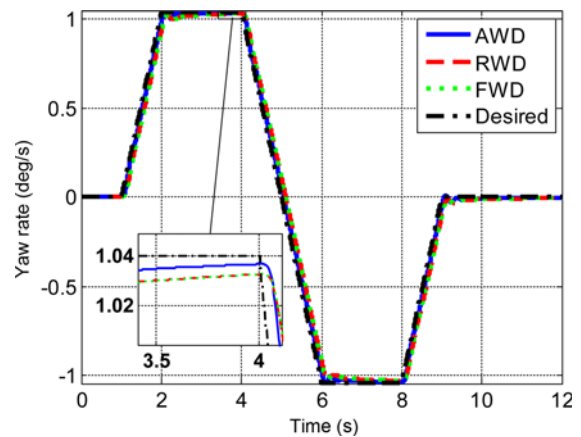


Figure 24. Yaw rate comparison results in the case of lane change simulations dry conditions.

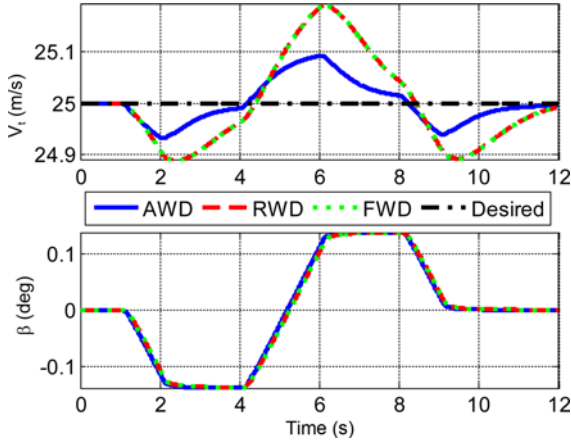


Figure 25. Vehicle total velocity, side-slip angle comparison results in the case of lane change simulations dry conditions.

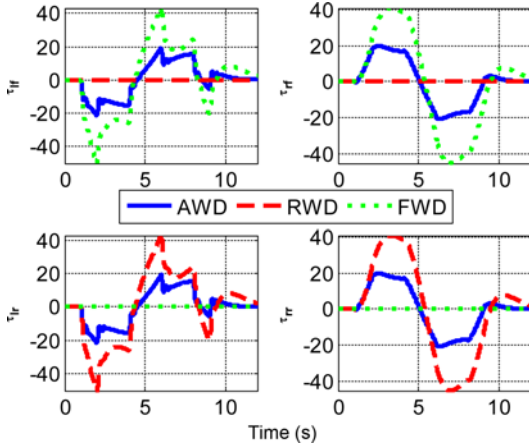


Figure 26. Control inputs comparison results in the case of lane change simulations dry conditions.

The yaw rate tracking also improved as compared to icy road conditions with no overshoots as shown in Figure 24.

Similar results are achieved for the velocity tracking with AWD outperforming the other two cases as shown in Figure 25. It is also noted that due to the dry road conditions the produced side-slip angle is very small as compared to icy road conditions.

The control inputs as shown in Figure 26, have similar behavior as discussed in the previous two cases.

Figure 27 shows the individual wheel's slip generated for the three sub cases. In this scenario due to the dry road conditions, the wheel's slip is the lowest for all cases. Due to small wheel's slip and large available friction due to dry conditions the EV will produce the best performance by tracking the velocity and desired yaw rate.

From the simulation results with dry road conditions it is also noted that in cases with good available friction between the wheels and road, the performance of the FWD

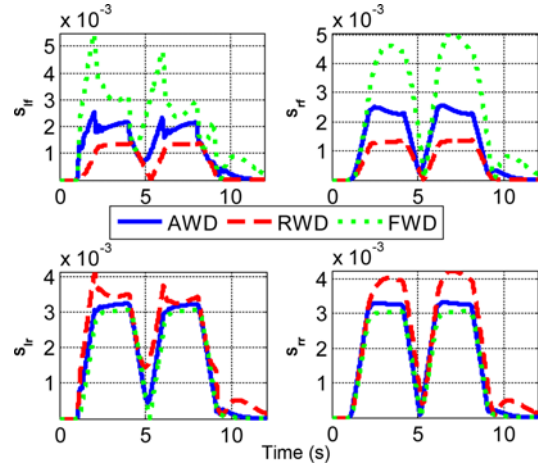


Figure 27. Wheel Slip comparison results in the case of lane change simulations dry conditions.

and RWD is similar but on icy road conditions with limited friction the COM of the vehicle plays the most important role in stability of vehicle. The AWD EV always produced the best stability performance on all road conditions.

5. CONCLUSION

In this study, a robust IA EV maneuvering system DSCS is investigated to maneuver the IA four wheel drive EV without the help of any CSM by utilizing the torque input of the four wheels. In this technique the functionality of the CSM is generated by using the differential speed of the left and right wheels of the IA EV. The DSCS achieved via H_∞ controller, is designed using the linear tire and vehicle model whereas the permanence is analyzed using full non-linear vehicle and tire model to mimic the real physical behavior. The effectiveness of the proposed control system is further analyzed by comparing the performance of FWD, RWD and AWD vehicles with DSCS during a J-turn and lane change maneuvers with different road conditions. From the results of the J-turn and lane change simulations it can be concluded that although DSCS can stabilize and track the desired maneuvers in all of the three tested cases but produces the best results in case of IA AWD EV by utilizing the torques of the four wheels.

ACKNOWLEDGEMENT—This study was supported by the BK21 plus Program funded by the Ministry of Education and National Research Foundation of South Korea (NRF).

REFERENCES

Bakker, E., Nyborg, L. and Pacejka, H. (1987). Tyre modelling for use in vehicle dynamics studies. *SAE Paper No. 870421*.
 Chen, B.-C. and Kuo, C.-C. (2014). Electronic stability control for electric vehicle with four in-wheel motors.

- Int. J. Automotive Technology* **15**, **4**, 573–580.
- Chen, Y. and Li, L. (2014). *Advances in Intelligent Vehicles*. Zhejiang University Press. China.
- Du, H., Zhang, N. and Dong, G. (2010). Stabilizing vehicle lateral dynamics with considerations of parameter uncertainties and control saturation through robust yaw control. *IEEE Trans. Vehicular Technology* **59**, **5**, 2593–2597.
- Glover, K. (1984). All optimal Hankel-norm approximations of linear multivariable systems and their L, ∞ -error bounds. *Int. J. Control* **39**, **6**, 1115–1193.
- Hori, Y. (2004). Future vehicle driven by electricity and control-research on four-wheel-motored “UOT electric march II”. *IEEE Trans. Industrial Electronics* **51**, **5**, 954–962.
- Hu, C., Wang, R., Yan, F. and Karimi, H. R. (2016). Robust composite nonlinear feedback path-following control for independently actuated autonomous vehicles with differential steering. *IEEE Trans. Transportation Electrification* **2**, **3**, 312–321.
- Jang, Y., Lee, M., Suh, I.-S. and Nam, K. (2017). Lateral handling improvement with dynamic curvature control for an independent rear wheel drive EV. *Int. J. Automotive Technology* **18**, **3**, 505–510.
- Kozłowski, K. and Pazderski, D. (2004). Modeling and control of a 4-wheel skid-steering mobile robot. *Int. J. Applied Mathematics and Computer Science* **14**, **4**, 477–496.
- Li, Q., Yu, X., Zhang, H. and Huang, R. (2015). Study on differential assist steering system with double in-wheel motors with intelligent controller. *Mathematical Problems in Engineering*, **2015**, Article ID 910230.
- McFarlane, D. C. and Glover, K. (1990). *Robust Controller Design Using Normalized Coprime Factor Plant Descriptions*. Springer-Verlag Berlin Heidelberg. Heidelberg, Germany.
- Ono, E., Hattori, Y., Muragishi, Y. and Koibuchi, K. (2006). Vehicle dynamics integrated control for four-wheel-distributed steering and four-wheel-distributed traction/braking systems. *Vehicle System Dynamics: Int. J. Vehicle Mechanics and Mobility* **44**, **2**, 139–151.
- Skogestad, S. and Postlethwaite, I. (1996). *Multivariable Feedback Control: Analysis and Design*. 2nd edn. Wiley. New York, USA.
- Wang, J., Wang, R., Jing, H. and Chen, N. (2016). Coordinated active steering and four-wheel independently driving/braking control with control allocation. *Asian Journal of Control* **18**, **1**, 98–111.
- Wang, R., Chen, Y., Feng, D., Huang, X. and Wang, J. (2011). Development and performance characterization of an electric ground vehicle with independently actuated in-wheel motors. *J. Power Sources* **196**, **8**, 3962–3971.
- Wong, J. Y. (1993). *Theory of Ground Vehicles*. John Wiley & Sons. Hoboken, New Jersey, USA.
- Wu, D., Ding, H. and Du, C. (2018). Dynamics characteristics analysis and control of FWID EV. *Int. J. Automotive Technology* **19**, **1**, 135–146.
- Wu, X., Xu, M. and Wang, L. (2013). Differential speed steering control for four-wheel independent driving electric vehicle. *Proc. IEEE Int. Symp. Industrial Electronics*, Taipei, Taiwan.
- Xiong, L. and Yu, Z. (2009). Control allocation of vehicle dynamics control for a 4 in-wheel-motored EV. *Proc. IEEE 2nd Int. Conf. Power Electronics and Intelligent Transportation System (PEITS)*, Shenzhen, China.
- Yi, J., Wang, H., Zhang, J., Song, D., Jayasuriya, S. and Liu, J. (2009). Kinematic modeling and analysis of skid-steered mobile robots with applications to low-cost inertial-measurement-unit-based motion estimation. *IEEE Trans. Robotics* **25**, **5**, 1087–1097.
- Yin, G., Wang, R. and Wang, J. (2015). Robust control for four wheel independently-actuated electric ground vehicles by external yaw-moment generation. *Int. J. Automotive Technology* **16**, **5**, 839–847.
- Youn, I., Wu, L., Youn, E. and Tomizuka, M. (2015). Attitude motion control of the active suspension system with tracking controller. *Int. J. Automotive Technology* **16**, **4**, 593–601.
- Yu, W., Chuy, O. Y., Collins, E. G. and Hollis, P. (2010). Analysis and experimental verification for dynamic modeling of a skid-steered wheeled vehicle. *IEEE Trans. Robotics* **26**, **2**, 340–353.
- Zhang, H., Zhang, X. and Wang, J. (2014a). Robust gain-scheduling energy-to-peak control of vehicle lateral dynamics stabilisation. *Vehicle System Dynamics: Int. J. Vehicle Mechanics and Mobility* **52**, **3**, 309–340.
- Zhang, L., Li, L., Lin, C., Wang, C., Qi, B. and Song, J. (2014b). Coaxial-coupling traction control for a four-wheel-independent-drive electric vehicle on a complex road. *Proc. Institution of Mechanical Engineers, Part D: J. Automobile Engineering* **228**, **12**, 1398–414.